INORGANIC CHEMISTRY FRONTIERS

RESEARCH ARTICLE

View Article Online
View Journal | View Issue

Cite this: *Inorg. Chem. Front.*, 2024, **11**, 3520

$NaVSeO_5$: synergistic combinations to synthesize excellent birefringent materials†

Qiuyuan Feng,‡[a] Jialong Wang,‡[b] Changyou Liu,[b] Qun Jing *[b] and Xiaoyu Dong *[c]

Received 28th February 2024,
Accepted 20th April 2024

DOI: 10.1039/d4qi00513a

rsc.li/frontiers-inorganic

Novel $NaVSeO_5$ birefringent crystals were successfully synthesized using a multifunctional group synergistic strategy, which combines a two-dimensional layered structure consisting of stereochemically active lone pairs [SeO_3] and anomalous [VO_6] polyhedra. Polarization microscopy tests reveal that $NaVSeO_5$ possesses significant birefringence (0.180@546 nm). Theoretical analysis suggests that this birefringence is attributed to the synergistic effect between highly distorted V–O polyhedra and stereochemically active lone pairs of Se^{4+}. Based on UV-Vis-NIR diffuse reflectance analysis, the crystal $NaVSeO_5$ demonstrates a cut-off edge below 336 nm. This study provides valuable insights for future exploration of novel birefringent crystal materials.

Introduction

Crystals with anisotropic arrangements of units have a broad spectrum of physical features, one of which is birefringence (Δn), a vital and essential optical property for optical materials.[1,2] It is essential to examine artificial crystals' birefringence in optical functional materials.[3–7] Birefringent crystal materials, a type of linear optical material, are widely used in high-precision scientific research tools, optical communication, and various other scientific and technological disciplines.[8,9] They are also capable of modulating and detecting the polarization state of light.[10,11] In recognition of their extraordinary properties, a variety of birefringent materials have been becoming more and more well-known in particular fields over the past few decades.[12,13]

There are some famous birefringent crystals available commercially, such as YVO_4 (0.208@1064 nm),[14,15] $CaCO_3$ (0.172@532 nm),[16] $LiNbO_3$ (0.074@546 nm),[17] α-BaB_2O_4 (0.122@546 nm),[18,19] and TiO_2 (0.256@1530 nm).[20] However, these materials still have some inherent limitations, like the relatively narrow band transmittance of YVO_4 and TiO_2[21,22] and the impurities of calcite.[23] As for α-BBO, the growing issue of phase transition is energy demanding and leads to the high cost of developing high quality single crystals.[24,25] In other words, existing crystal materials struggle to meet the evolving practical needs of societal development. The creation of birefringent crystals with substantial optical anisotropy for use in optical elements is consequently of tremendous scientific and technological relevance.[26–29]

To design and synthesize novel compounds with large birefringence, lots of literature reports have been investigated. V–O anionic groups were first chosen because V–O contributes up to 70% to the birefringence of the commercial material YVO_4.[30] Additionally, $Sn_2B_5O_9X$ (X = Cl and Br)[31,32] has enhanced birefringence compared with the isostructural $M_2B_5O_9X$ (M = Ca, Sr, Ba, and Eu, X = Cl, Br, and I). Its birefringence is shown to be mostly attributed to the stereochemically active lone pair (SCALP) cation. So stereochemically active lone pair (SCALP) cations such as Te^{4+}, Sn^{2+}, and Se^{4+} could be selected[33–37] to achieve higher birefringence. Furthermore, transition metals having d^0 electronic configuration (d^0 TM), such as V^{5+}, Nb^{5+}, and Mo^{6+}, are also favourable to the birefringence due to second-order Jahn–Teller (SOJT) distortions and the distortion degree of the d^0-TM centered polyhedron.[38–41]

Based on these ideas, our research focuses on combining hybrid anionic functional building blocks containing the stereochemically active component Se^{4+} and susceptible to SOJT distortion V^{5+} octahedra into a single structure. This approach is used to enhance optical anisotropy in the quest for birefringent materials with a short cut-off edge and superior birefringence. After numerous attempts, a novel $NaVSeO_5$ birefringent material (Δn = 0.180@546 nm) was suc-

[a]*College of Chemistry and Chemical Engineering, Xinjiang Normal University, Urumqi, Xinjiang 830054, P. R. China*
[b]*School of Physical Science and Technology, Xinjiang University, 777 Huarui Road, Urumqi, 830017, P. R. China. E-mail: qunjing@xju.edu.cn*
[c]*Engineering Department of Chemistry and Environment, Xinjiang Institute of Engineering, Urumqi, Xinjiang 830091, P. R. China. E-mail: dxy@xjie.edu.cn*

†Electronic supplementary information (ESI) available: CIF files, atomic coordinates, equivalent isotropic displacement parameters and bond valence sum (BVS) and the table of bond lengths and angles for $NaVSeO_5$. CCDC 2334821. For ESI and crystallographic data in CIF or other electronic format see DOI: https://doi.org/10.1039/d4qi00513a

‡These authors contributed equally to this work.

cessfully synthesized. Its synthesis, crystal structure, UV-visible-near-infrared diffuse reflectance spectra, and vibrational spectra are reported in this paper. In addition, the first principles result reveals that its large birefringence originates from the VO radical and the SeO moiety.

Experimental

Reagents

The starting agents Na_2CO_3, (Tianjin BaiShi Chemical Co., Ltd, 99.8%), SeO_2, (Aladdin Chemical Industry Co., Ltd, 99.0%), and V_2O_5, (Beijing Chemical Industry Co., Ltd, 99.0%) were used as received without any further treatment.

Single crystal growth

$NaVSeO_5$ crystals were obtained for the first time in a sealed environment. The raw materials Na_2CO_3, SeO_2, and V_2O_5 in a molar ratio of 1 : 1 : 9 were placed in a clean and dry quartz tube (Φ 10 mm × 100 mm). The quartz tube was pumped to a high vacuum of 10^{-3} Pa and sealed and then put into a muffle furnace and heated from room temperature to 450 °C for 13 h and held for half a day. Subsequently, it was slowly cooled to 280 °C at 2 °C h^{-1} and then to 25 °C at a rate of 5 °C h^{-1}. Single crystals of $NaVSeO_5$ were manually selected after opening the quartz glass tube.

Single crystal X-ray crystallography studies

The small colorless single crystals of $NaVSeO_5$ of 0.17 × 0.14 × 0.12 mm^3 were stuck to a glass fiber to record the crystal structure data using an APEX II CCD X-ray diffractometer equipped with monochromatic Mo–Kα radiation at 296 K. The absorption corrections and data integration were achieved using the SAINT program. The structure was solved by direct methods using the SHELXTL crystallographic program, and the full matrix least-squares techniques were applied to refine the position of all the atoms.[42–46] Finally, we acquired $NaVSeO_5$ crystal structures with a degree of completeness of more than 99%. Table 1 shows the crystal data and structure refinement of $NaVSeO_5$. The PLATON program was used to verify the symmetry of the structure.[47] The atomic coordinates, bond valence sums (BVS), selected bond lengths (Å), and bond angles are shown in Tables S1–S3 in the ESI†.

Solid-state synthesis

The polycrystals of the title compounds were synthesized by solid-state reactions of Na_2CO_3 SeO_2, and V_2O_5 in a 1 : 1 : 1 molar ratio. Compound $NaVSeO_5$ was synthesized by heating a homogeneous mixture of the samples to 120 °C, annealing for 7 h, and then heating the samples to 350 °C and maintaining them for 8 h through multiple intermediate grinding and mixing.

Powder X-ray diffraction

The purity of polycrystalline $NaVSeO_5$ was confirmed using a Bruker D2 PHASER X-ray diffractometer with Cu Kα radiation (λ = 1.5418 Å). The diffraction data were collected in the range of 5–120° (2θ) with a fixed counting time and a scan step width of 1 s per step and 0.02°, respectively. The diffraction pattern agrees well with the theoretical one, as shown in Fig. 1a.

Table 1 Crystal data and structure refinement for $NaVSeO_5$

Empirical formula	$NaVSeO_5$
Formula weight	232.89 g mol^{-1}
Crystal system	Monoclinic
Space group, Z	$C2/c$, 8
Unit cell dimensions (Å)	a = 18.234(3) b = 3.8381(6), β = 112.421(7) c = 12.416(2)
Volume	803.2(2) $Å^3$
Density (calc.)	3.852 g cm^{-3}
$F(000)$	864
θ range for data collection	2.42 to 27.52°
Limiting indices	$-23 \le h \le 23$, $-4 \le k \le 4$, $-16 \le l \le 16$
Reflections collected	6766
Independent reflections	2478 [R_{int} = 0.0645]
Data/restraints/parameters	910/0/73
Completeness to θ (%)	99.9%
Refinement method	Full-matrix least-squares on F^2
Goodness of fit on F^2	1.066
Final R indices [$F_o^2 > 2\delta(F_o^2)$][a]	R_1 = 0.0317, wR_2 = 0.0652
R indices (all data)[a]	R_1 = 0.0407, wR_2 = 0.0698
The largest diff. peak and hole	0.895 and −1.042 e·$Å^{-3}$

[a] $R_1 = \sum||F_o| - |F_c||/\sum|F_o|$ and $wR_2 = [\sum w(F_o^2 - F_c^2)^2/\sum wF_o^4]^{1/2}$ for $F_o^2 > 2\sigma(F_o^2)$.

Rietveld refinement

The polycrystals were obtained directly by grinding the obtained crystals and the Rietveld refinement[48] was used to verify the correctness of the solved structure and the purity of the samples (shown in Fig. 1a). The fit curves match the experimental data obtained from the single-crystal CIF data, leading to reasonable R values of W_R = 0.0877 and R_p = 0.0576, respectively, and all observed Bragg reflections are indexed to the $C2/c$ space group, respectively.

EDS analysis

Energy dispersive X-ray spectroscopy (EDS) was carried out on a clean single-crystal surface with the aid of a field emission scanning electron microscope (SUPRA 55VP) equipped with an

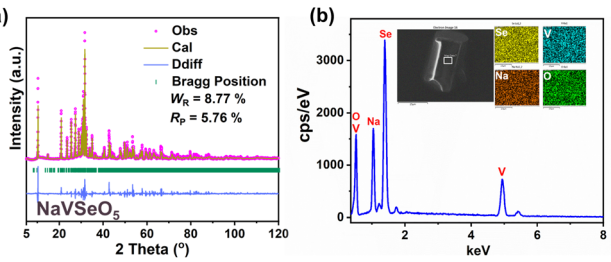

Fig. 1 (a) Rietveld refinement of the powder X-ray diffraction pattern of compound $NaVSeO_5$ polycrystals. A full Rietveld refinement was carried out using GSAS II software. (b) EDS maps of Na, V, Se, and O in the compound crystal. Scale bar is 2.5 μm.

energy dispersive X-ray spectrometer (Bruker xflash-sdd-5010). Additionally, EDS was conducted on a $NaVSeO_5$ single crystal, confirming the presence of the corresponding elements within the compound (shown in Fig. 1b).

UV–Vis–NIR diffuse reflectance measurement

To determine the cutoff edge of the title crystal, the UV–Vis–NIR diffuse reflectance spectrum was recorded. The diffuse reflectance spectrum was recorded at room temperature with a Shimadzu SolidSpec-3700DUV spectrophotometer.[49,50]

IR spectroscopy

The infrared (IR) spectrum was recorded to specify the coordination of the V and Se atoms. The IR spectrum was recorded on a Shimadzu IRAffinity-1 Fourier transform IR spectrometer in the range of 400–4000 cm^{-1}. The sample was mixed thoroughly with dried KBr.[51]

Thermal analyses

Thermal gravimetry (TG) and differential scanning calorimetry (DSC) were carried out to examine the thermal stability of $NaVSeO_5$ on a simultaneous NETZSCH STA 449 F3 thermal analyzer instrument under a flowing N_2 atmosphere. The sample was placed in a Pt crucible and heated from 40 to 800 °C at a rate of 5 °C min^{-1}.

Birefringence

The refractive index difference of $NaVSeO_5$ was characterized by using a polarizing microscope equipped (ZEISS Axio Scope. A1) with a Berek compensator. The refractive index difference of the crystal at 546 nm was calculated using the equation $R = \Delta n \times d$, where R, Δn, and d denote retardation, the refractive index difference, and thickness, respectively. The natural growth plane of the crystals does not always align with a specific optical principal axis, so the measured refractive index difference is smaller than the actual birefringence. In that sense, the birefringence of $NaVSeO_5$ should be close to or larger than the test value.[52]

Theoretical computations

In an effort to further explore the factors influencing the optical properties of crystals, the electronic structures and optical properties of $NaVSeO_5$ were analysed using the CASTEP[53] code based on density functional theory (DFT).[54,55] During the calculation, the exchange–correction functional was selected with Perdew–Burke–Ernzerhof (PBE)[56] in the generalized gradient approximation (GGA). Geometry optimization was performed, and the tolerance of total energy, max. ionic force, max. ionic displacement, and max. stress are set as 5×10^{-6} eV per atom, 1×10^{-1}eV $Å^{-1}$, 5×10^{-4} Å and 2×10^{-2} GPa, respectively. The core electrons are treated using Norm-Conserving Pseudopotentials (NCP),[57,58] and the valence electrons are set as Na $2s^2$ $2p^6$ $3s^1$, V $3d^3$ $4s^2$, Se $4s^2$ $4p^4$, and O $2s^2$ $2p^4$. The plane-wave energy cutoff was set at 830 eV and the separation of the k-point was set as 0.04 $Å^{-1}$ in the $7 \times 7 \times 2$ Brillouin zone. The other calculation parameters and convergent criteria were set as the default values of the CASTEP code. After obtaining the electronic structure, the refractive indices and birefringence were further calculated using the OptaDOS[59,60] code. The functional basic units' contribution to the optical response is analysed using the real-space atom-cutting (RSAC) method.[61]

Results and discussion

Crystal structure

Analysis of single crystal diffraction data reveals that $NaVSeO_5$ adopts a monoclinic crystal system with a centrosymmetric space group of $C2/c$ (no. 15) (shown in Table 1). The asymmetric unit of the structure comprises one Na, one V, one Se, and five independent O atoms (shown in Table S1†). The crystal structure of $NaVSeO_5$ is characterized by 2D layers, which are composed of isolated trigonal pyramid $[SeO_3]$ groups and 1D $[VO_4]_\infty$ infinite chains (shown in Fig. 2c). The V atoms are connected by oxygen atoms, forming $[VO_6]$ distorted octahedra, while the Se atoms are coordinated with three oxygen atoms to create trigonal pyramid $[SeO_3]$ groups (shown in Fig. 2a). In order to accurately represent the distortions of $[VO_6]$ and $[SeO_3]$, the distortions were evaluated using the Baur method implemented in the VESTA code.[62,63] The distortions (Δd) are 0.119 and 0.027, respectively. Notably, the bond lengths and angles within the $NaVSeO_5$ structure closely resemble the structures found in previously reported vanadate-selenites (shown in Table S4†).[64,65] Initially, these $[VO_6]$ octahedra have consistent deformation directions and are assembled into one-dimensional $[VO_4]_\infty$ infinite chains by sharing an edge along the c-axis. Therefore, this is conducive to the production of large birefringence (as shown in Fig. 2b). Subsequently, the aforementioned 1D $[VO_4]_\infty$ infinite chains are linked together by isolated $[SeO_3]$ groups, resulting in the assembly of 2D $[SeVO_5]_\infty$ infinite layers that extend along the bc-plane (shown in Fig. 2c). Finally, the 2D $[SeVO_5]_\infty$ infinite layers were bound through Na–O ionic bonds and stacked along the a-axis (shown in Fig. 2d).

Spectroscopy analyses

UV-Vis-NIR diffuse reflectance spectroscopy showed that the crystal of $NaVSeO_5$ had almost no absorption in the range of 336 to 2500 nm.

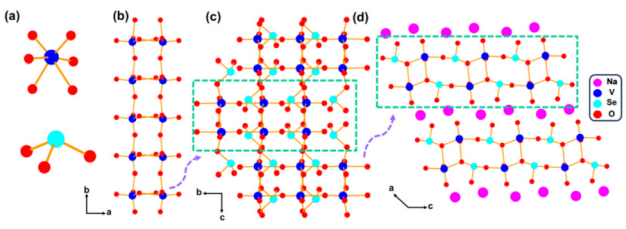

Fig. 2 (a) The $[VO_6]$ octahedron and the trigonal pyramid $[SeO_3]$ group. (b) 1D $[VO_4]_\infty$ chain. (c) View of the 2D $[VSeO_5]_\infty$ layer along the bc-plane. (d) The whole structure of $NaVSeO_5$ is viewed along the b-axis.

The experimental band gap values of the crystals of $NaVSeO_5$ indicate almost no absorption in the range of 336 to 2500 nm. The experimental band gap values of the $NaVSeO_5$ were obtained at about 2.36 eV (shown in Fig. 3a). The IR spectra of compound $NaVSeO_5$ were measured in the 400–4000 cm^{-1} wavenumber range at room temperature (shown in Fig. 3b). The infrared spectra of the compound exhibit both V–O and Se–O vibrations. The absorption band in the range of 764–930 cm^{-1} can be classified as V–O bond vibration. The absorption band in the range of 526–620 cm^{-1} as Se–O bond vibration is consistent with previously reported data.[66–68]

Thermal analyses

As shown in Fig. S1,† the thermogram indicates that the title compound has a continuous weight loss at intervals of 315 °C with slope changes. These weight losses correspond to the release of the SeO_2. Thermal behavior analysis and powder X-ray diffraction (XRD) data at various temperatures indicate that $NaVSeO_5$ remains thermally stable above 400 °C under open conditions (as shown in Fig. S2†).

Birefringence analysis

A high-quality crystal was intentionally selected to ensure more accurate birefringence measurements. The crystal reached extinction when the Berek compensator's drum was reversed, and the corresponding values were recorded. According to the Berek compensator's specification tables, the thickness of the selected crystals was 9.92 μm, and the optical path difference at 546 nm was 1.859 μm. The refractive index difference of $NaVSeO_5$ is 0.180@546 nm. The refractive index difference is known to be measured on the (100) crystal plane (shown in Fig. 4d). The experimental measurements range from zero to the birefringence value, as Δn represents the maximum refractive index difference. Comparison with other crystals in the same wavelength band reveals that the compound exhibits significant birefringence (shown in Fig. S3 and Table S5†).

Theoretical calculations and optical properties

To study the structure–property relationship of $NaVSeO_5$, first-principles calculations were used to analyze its electronic structures (shown in Fig. 5). It is clearly shown that $NaVSeO_5$ has an indirect band gap, and the theoretical band gap is about 1.87 eV, which is less than the value (2.36 eV) obtained from the transmittance spectrum (shown in Fig. 5a). The underestimation of the band gap drives from the inaccurately described unoccupied eigenvalues of electronic states.[69] Usually, the states near the band gap control the optical properties of a crystal, so the valence-band maximum (VBM) and the conduction band minimum (CBM) were carefully studied in the PDOS. The obtained PDOS is shown in Fig. 5b, the PDOS graph is divided into VB-I–II and CB energy regions. Se-4p and O-2p states dominate the VB-I region. O-2p and V 3d electronic states occupy VB-II. In CB, it is dominated by O-2p, V-3d, and Se-4p electronic states. Both VBM and CBM are mainly from the electronic states of V–O and Se–O. Additionally, we evaluated the birefringence of $NaVSeO_5$ through theoretical calculations. Fig. 5c indicates that the birefringence of $NaVSeO_5$ is about 0.189 at 546 nm. The birefringence values calculated for $NaVSeO_5$ are in good agreement with experimental data.

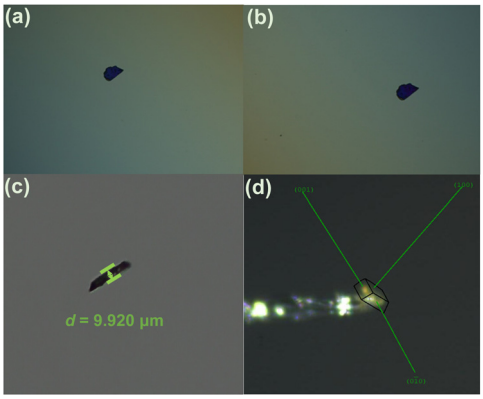

Fig. 4 (a and b) Extinction views of the crystal by negative and positive rotational compensators; (c) view of the crystal thickness; (d) orientation of the $NaVSeO_5$ crystal determined by X-ray single-crystal diffraction.

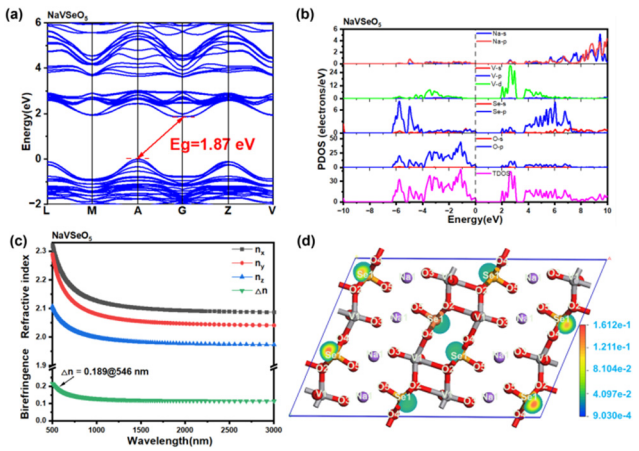

Fig. 5 (a) The birefringence of compound $NaVSeO_5$; (b) partial density of states (PDOS) of compound $NaVSeO_5$; (c) calculated band structure; (d) ELF of compound $NaVSeO_5$.

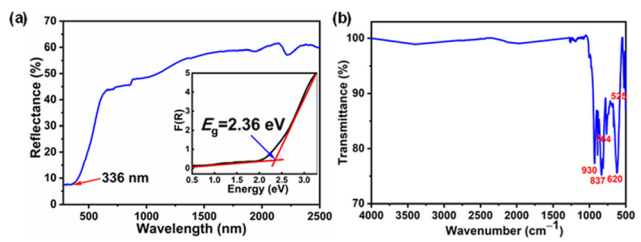

Fig. 3 (a) UV-Vis-NIR diffuse reflectance and absorption spectra of $NaVSeO_5$; (b) IR spectrum of $NaVSeO_5$.

Table 2 The functional basic units' refractive indices and birefringence were obtained by RSAC methods

Compound		n_x	n_y	n_z	Δn
$NaVSeO_5$	Origin	2.269	2.229	2.080	0.189
	SeO_3	2.054	1.834	1.833	0.221
	VO_6	2.047	1.914	1.852	0.195

The RSAC method was used to further investigate the contributions of different groups to the refractive indices and birefringence. In the RSAC operation, the atomic radii were set according to the rule of keeping the cutting spheres in contact but without overlapping, and these values were set as 1.095 Å (Na), 0.98 Å (V), 1.82 Å (Se), and 1.10 Å (O). The obtained RSAC results are shown in Table 2, the birefringence of the Se–O polyhedral (0.221@546 nm) is larger than that of V–O (0.195@546 nm) polyhedra in $NaVSeO_5$, implying that Se–O polyhedra with asymmetric lone pair electrons give more contribution to total birefringence. The asymmetric lone pair electrons are further confirmed by the electron localization function (ELF). ELF intuitively reveals that there is a lobe-like isosurface around the Se^{4+} atom, which illustrates that lone pairs of Se^{4+} are stereochemically active (shown in Fig. 5d). Hence, it suggests that $NaVSeO_5$ has large anisotropic polarizabilities and birefringence.

Conclusions

In conclusion, a novel inorganic compound $NaVSeO_5$ with excellent birefringence properties has been successfully developed in a closed system using a synergistic strategy that involves multifunctional groups. In the structure of $NaVSeO_5$, the $[VO_4]_\infty$ infinite chain is linked to isolated $[SeO_3]$ groups, forming a regularly arranged two-dimensional $[SeVO_5]_\infty$ infinite layer. Due to the strong SCALP effect of Se^{4+}, the $[VO_6]$ octahedra have a consistent deformation direction, giving the compound a significant birefringence (0.180 at 546 nm). UV-visible-near-infrared diffuse reflectance spectroscopy reveals that $NaVSeO_5$ has a broad transmission range with a cut-off edge below 336 nm. This study enriches the selenite family and offers insights for the exploration of novel birefringent crystals.

Conflicts of interest

There are no conflicts to declare.

Acknowledgements

This work is supported by the Major Science and Technology Projects of Xinjiang (Grant No. 2022A01005), the National Natural Science Foundation of China (12264047), and the Tianshan Talent Project of Xinjiang Uygur Autonomous Region of China (2022TSYCJU0004).

References

1 Z. Chen, Z. Zhang, R. Wu, X. Dong, Y. Shi and Q. Jing, Theoretical study on $Pb_2VO_2F_5$: large birefringence derived from optical anisotropies of VO_2F_4 groups, *J. Mater. Sci.*, 2018, **53**, 3483–3492.
2 F. Liang, L. Kang, Z. Lin, Y. Wu and C. Chen, Analysis and prediction of mid-IR nonlinear optical metal sulfides with diamond-like structures, *Coord. Chem. Rev.*, 2017, **333**, 57–70.
3 X. L. Chen, B. B. Zhang, F. F. Zhang, Y. Wang, M. Zhang, Z. H. Yang, K. R. Poeppelmeier and S. L. Pan, Designing an excellent deep-ultraviolet birefringent material for light polarization, *J. Am. Chem. Soc.*, 2018, **140**, 16311–16319.
4 S. J. Yu, H. P. Wu, H. W. Yu, Z. G. Hu, J. Y. Wang and Y. C. Wu, $NH_4(B_6PO_{10}(OH)_4)\cdot H_2O$: exhibiting the largest birefringence in borophosphates, *Chem. Commun.*, 2022, **58**, 2834–2837.
5 M. G. Gao, Q. Bian, H. P. Wu, H. W. Yu, Z. G. Hu, J. Y. Wang and Y. C. Wu, Inducing large birefringence by enhancing asymmetric electron distribution of Y-O polyhedra, *Inorg. Chem. Front.*, 2022, **9**, 1956–1963.
6 M. M. Zhu, J. B. Wang, L. Hou, Y. W. Yuan, L. L. Liu, Y. Q. Chu and C. M. Huang, $AX\cdot(H_2SeO_3)_n$(A = K, Cs; X = Cl, Br; n = 1, 2): A Series of Ionic Cocrystals as Promising UV Birefringent Materials with Large Birefringence and Wide Band Gap, *Inorg. Chem.*, 2024, **63**, 2289–2297.
7 L. Yang, X. L. Chen and K. M. Ok, $KF\cdot B(OH)_3$: a KBBF-type material with large birefringence and remarkable deep-ultraviolet transparency, *Chem. Commun.*, 2022, **58**, 8770–8773.
8 S. Niu, G. Joe, H. Zhao, Y. Zhou, T. Orvis, H. Huyan, J. Salman, K. Mahalingam, B. Urwin, J. Wu, Y. Liu, T. E. Tiwald, S. B. Cronin, B. M. Howe, M. Mecklenburg, R. Haiges, D. J. Singh, H. Wang, M. A. Kats and J. Ravichandran, Giant optical anisotropy in a quasi-one-dimensional crysta, *Nat. Photonics*, 2018, **12**, 392–396.
9 F. Qin and R. K. Li, Predicting refractive indices of the borate optical crystals, *J. Cryst. Growth*, 2011, **318**, 642–644.
10 P. Hlubina, D. Ciprian and L. Knyblová, Interference of white light in tandem configuration of birefringent crystal and sensing birefringent fiber, *Opt. Commun.*, 2006, **260**, 535–541.
11 M. Li, H. F. Pan, Y. Q. Tong, C. Chen and H. P. Zeng, All-optical ultrafast polarization switching of terahertz radiation by impulsive molecular alignment, *Opt. Lett.*, 2011, **36**, 3633–3635.
12 M. F. Weber, C. A. Stover, L. R. Gilbert, T. J. Nevitt and A. J. Ouderkirk, Giant birefringent optics in multilayer polymer mirrors, *Science*, 2000, **287**, 2451–2456.
13 F. Flossmann, U. T. Schwarz, M. Maier and M. R. Dennis, Polarization singularities from unfolding an optical vortex through a birefringent crystal, *Phys. Rev. Lett.*, 2005, **95**, 253901.
14 L. G. DeShazer, Improved midinfrared polarizers using yttrium vanadate, *Proc. SPIE*, 2002, **4481**, 10–16.

15 C. Z. Bi, J. Y. Ma, J. Yan, X. Fang, D. Z. Yao, B. R. Zhao and X. G. Qiu, Far-infrared optical properties of YVO_4 single crystal, *Eur. Phys. J. B*, 2006, **51**, 167–171.
16 G. Ghosh, Dispersion-equation coefficients for the refractive index and birefringence of calcite and quartz crystals, *Opt. Commun.*, 1999, **163**, 95–102.
17 D. E. Zelmon, D. L. Small and D. Jundt, Infrared corrected Sellmeier coefficients for congruently grown lithium niobate and 5 mol% magnesium oxide–doped lithium niobate, *J. Opt. Soc. Am. B*, 1997, **14**, 3319–3322.
18 G. Q. Zhou, J. Xu, X. D. Chen, H. Y. Zhong, S. T. Wang, K. Xu, P. Z. Deng and F. X. Gan, Growth and spectrum of a novel birefringent α-BaB_2O_4 crystal, *J. Cryst. Growth*, 1998, **191**, 517–519.
19 V. P. Solntsev, E. G. Tsvetkov, V. A. Gets and V. D. Antsygin, Growth of α-BaB_2O_4 single crystals from melts at various compositions: comparison of optical properties, *J. Cryst. Growth*, 2002, **236**, 290–296.
20 J. R. DeVore, Refractive indices of rutile and sphalerite, *J. Opt. Soc. Am. A*, 1951, **41**, 416–419.
21 H. Zhang, X. Meng, L. Zhu, C. Wang, Y. T. Chow and M. Lu, Growth, spectra and influence of annealing effect on laser properties of Nd: YVO_4 crystal, *Opt. Mater.*, 2000, **14**, 25–30.
22 Y. F. Chen, L. J. Lee, T. M. Huang and C. L. Wang, Study of high-power diode-end-pumped Nd: YVO_4 laser at 1.34 μm: influence of Auger upconversion, *Opt. Commun.*, 1999, **163**, 198–202.
23 M. Simoni, T. Hanein, C. L. Woo, J. Provis and H. Kinoshita, Effect of Impurities on the Decarbonization of Calcium Carbonate Using Aqueous Sodium Hydroxide, *ACS Sustainable Chem. Eng.*, 2022, **10**, 11913–11925.
24 H. Zhang, M. Zhang, S. L. Pan, Z. H. Yang, Z. Wang, Q. Bian, X. L. Hou, H. W. Yu, F. F. Zhang, K. Wu, F. Yang, Q. J. Peng, Z. Y. Xu, K. B. Chang and K. R. Poeppelmeier, Next generation of deep-ultraviolet birefringent materials, *Cryst. Growth Des.*, 2015, **15**, 523–529.
25 S. F. Wu, G. F. Wang, J. L. Xie, Y. F. Zhang and X. Lin, Growth of large birefringent α-BBO crystal, *J. Cryst. Growth*, 2002, **245**, 84–86.
26 J. R. DeVore, Refractive Indices of Rutile and Sphalerite, *J. Opt. Soc. Am. A*, 1951, **41**, 416–419.
27 M. Zhang, D. H. An, C. Hu, X. L. Chen, Z. H. Yang and S. L. Pan, Rational design via synergistic combination leads to an outstanding deep-ultraviolet birefringent $Li_2Na_2B_2O_5$ material with an unvalued B_2O_5 functional gene, *J. Am. Chem. Soc.*, 2019, **141**, 3258–3264.
28 D. Zhang, Q. Wang, T. Zheng, L. L. Cao, K. M. Ok, D. J. Gao, J. Bi, L. Huang and G. H. Zou, Cation-anion synergetic interactions achieving tunable birefringence in quasi-one-dimensional antimony(III) fluoride oxalates, *Sci. China Mater.*, 2022, **65**, 3115–3124.
29 Y. Hou, B. B. Zhang, H. P. Wu, H. W. Yu, Z. G. Hu, J. Y. Wang and Y. C. Wu, $K_3B_4PO_{10}$ and $K_2MB_4PO_{10}$ (M = Rb/Cs): rare mixed-coordinated borophosphates with large birefringence, *Inorg. Chem. Front.*, 2021, **8**, 1468–1475.
30 B. H. Lei, Z. H. Yang and S. L. Pan, Enhancing optical anisotropy of crystals by optimizing bonding electron distribution in anionic groups, *Chem. Commun.*, 2017, **53**, 2818–2821.
31 J. Y. Guo, S. C. Cheng, S. J. Han, Z. H. Yang and S. L. Pan, $Sn_2B_5O_9Br$ as an Outstanding Bifunctional Material with Strong Second–Harmonic Generation Effect and Large Birefringence, *Adv. Opt. Mater.*, 2021, **9**, 2001734.
32 J. Y. Guo, A. Tudi, S. J. Han, Z. H. Yang and S. L. Pan, $Sn_2B_5O_9Cl$: A Material with Large Birefringence Enhancement Activated Prepared via Alkaline–Earth–Metal Substitution by Tin, *Angew. Chem., Int. Ed.*, 2019, **58**, 17675–17678.
33 J. B. Wang, M. M. Zhu, Y. Q. Chu, J. D. Tian, L. L. Liu, B. B. Zhang and P. S. Halasyamani, Rational Design of the Alkali Metal Sn–Based Mixed Halides with Large Birefringence and Wide Transparent Range, *Small*, 2023, 2308884.
34 J. Y. Guo, A. Tudi, S. J. Han, Z. H. Yang and S. L. Pan, α–SnF_2: a UV birefringent material with large birefringence and easy crystal growth, *Angew. Chem., Int. Ed.*, 2021, **60**, 3540–3544.
35 Y. C. Liu, X. M. Liu, S. Liu, Q. R. Ding, Y. Q. Li, L. N. Li, S. G. Zhao, Z. S. Lin, J. H. Luo and M. C. Hong, An unprecedented antimony(III) borate with strong linear and nonlinear optical responses, *Angew. Chem., Int. Ed.*, 2020, **59**, 7793–7796.
36 H. Wang, L. L. Liu, Z. W. Hu, J. B. Wang, M. M. Zhu, Y. Meng and J. Y. Xu, $RbCl{\cdot}(H_2SeO_3)_2$: A Salt-Inclusion Selenite Featuring Short UV Cut-Off Edge and Large Birefringence, *Inorg. Chem.*, 2022, **62**, 557–564.
37 Y. Yang, Y. Qiu, P. F. Gong, L. Kang, G. M. Song, X. M. Liu, J. L. Sun and Z. S. Lin, Lone–Pair Enhanced Birefringence in an Alkaline–Earth Metal Tin(II) Phosphate $BaSn_2(PO_4)_2$, *Chem. – Eur. J.*, 2019, **25**, 5648–5651.
38 E. O. Chi, K. M. Ok, Y. Porter and P. S. Halasyamani, $Na_2Te_3Mo_3O_{16}$: A new molybdenum tellurite with second-harmonic generating and pyroelectric properties, *Chem. Mater.*, 2006, **18**, 2070–2074.
39 H. S. Ra, K. M. Ok and P. S. Halasyamani, Combining second-order Jahn-Teller distorted cations to create highly efficient SHG materials: synthesis, characterization, and NLO properties of $BaTeM_2O_9$ (M = Mo^{6+} or W^{6+}), *J. Am. Chem. Soc.*, 2003, **125**, 7764–7765.
40 J. J. Zhang, Z. H. Zhang, Y. X. Sun, C. Q. Zhang, S. J. Zhang, Y. Liu and X. T. Tao, $MgTeMoO_6$: A neutral layered material showing strong second-harmonic generation, *J. Mater. Chem.*, 2012, **22**, 9921–9927.
41 R. Gautier, R. Gautier, K. B. Chang and K. R. Poeppelmeier, On the Origin of the Differences in Structure Directing Properties of Polar Metal Oxyfluoride $[MO_xF_{6-x}]^{2-}$(x = 1, 2) Building Units, *Inorg. Chem.*, 2015, **54**, 1712–1719.
42 M. Shang and P. S. Halasyamani, Mixed-valent selenium compounds: Noncentrosymmetric $Cd_3(SeO_3)_2(SeO_4)$ and $Hg_3(SeO_3)_2(SeO_4)$ and centrosymmetric $Pb_2(SeO_3)(SeO_4)$, *J. Solid State Chem.*, 2020, **286**, 121292.

43 L. L. Liu, B. B. Zhang, P. S. Halasyamani and W. G. Zhang, a new polar compound with the strongest second harmonic generation in the selenite bromide family, *J. Mater. Chem. C*, 2021, **9**, 6491–6497.

44 L. T. Menezes, E. Gage, A. Assoud, M. Liang, P. S. Halasyamani and H. Kleinke, $Sr_6Ge_3OSe_{11}$: A Rationally Designed Noncentrosymmetric Oxyselenide with Polar [$GeOSe_3$] Building Blocks, *Chem. Mater.*, 2023, **35**, 3033–3040.

45 G. Q. Shi, Y. Wang, F. F. Zhang, B. B. Zhang, Z. H. Yang, X. L. Hou, S. L. Pan and K. R. Poeppelmeier, Finding the next deep-ultraviolet nonlinear optical material: $NH_4B_4O_6F$, *J. Am. Chem. Soc.*, 2017, **139**, 10645–10648.

46 B. B. Zhang, G. Q. Shi, Z. H. Yang, F. F. Zhang and S. L. Pan, Fluorooxoborates: beryllium–free deep–ultraviolet nonlinear optical materials without layered growth, *Angew. Chem., Int. Ed.*, 2017, **56**, 3916–3919.

47 A. L. Spek, Single-crystal structure validation with the program PLATON, *J. Appl. Crystallogr.*, 2003, **36**, 7.

48 X. F. Wang, Y. Wang, B. B. Zhang, F. F. Zhang, Z. H. Yang and S. L. Pan, a congruent–melting deep–ultraviolet nonlinear optical material by combining superior functional units, *Angew. Chem., Int. Ed.*, 2017, **56**, 14119–14123.

49 Y. Wang, B. B. Zhang, Z. H. Yang and S. L. Pan, Cation–tuned synthesis of fluorooxoborates: towards optimal deep–ultraviolet nonlinear optical materials, *Angew. Chem., Int. Ed.*, 2018, **57**, 2150–2154.

50 M. Mutailipu, M. Zhang, H. P. Wu, Z. H. Yang, Y. H. Shen, J. L. Sun and S. L. Pan, $Ba_3Mg_3(BO_3)_3F_3$ polymorphs with reversible phase transition and high performances as ultraviolet nonlinear optical materials, *Nat. Commun.*, 2018, **9**, 3089.

51 J. P. Perdew, K. Burke and M. Ernzerhof, Generalized gradient approximation made simple, *Phys. Rev. Lett.*, 1996, **77**, 3865–3868.

52 L. L. Cao, G. Peng, W. B. Liao, T. Yan, X. F. Long and N. Ye, A microcrystal method for the measurement of birefringence, *CrystEngComm*, 2020, **22**, 1956–1961.

53 S. J. Clark, M. D. Segall, C. J. Pickard, P. J. Hasnip, M. J. Probert, K. Rrfson and M. C. Payne, First principles methods using CASTEP, *Z. Kristallogr.*, 2005, **220**, 567.

54 B. H. Lei, S. L. Pan, Z. H. Yang, C. Cao and D. J. Singh, Second harmonic generation susceptibilities from symmetry adapted Wannier functions, *Phys. Rev. Lett.*, 2020, **125**, 187402.

55 D. Vanderbilt, Soft self-consistent pseudopotentials in a generalized eigenvalue formalism, *Phys. Rev. B: Condens. Matter Mater. Phys.*, 1990, **41**, 7892.

56 J. P. Perdew, K. Burke and M. Ernzerhof, Generalized gradient approximation made simple, *Phys. Rev. Lett.*, 1996, **77**, 3865–3868.

57 L. Kleinman and D. M. Bylander, Efficacious form for model pseudopotentials, *Phys. Rev. Lett.*, 1982, **48**, 1425–1428.

58 D. R. Hamann, M. Schlüter and C. Chiang, Norm-conserving pseudopotentials, *Phys. Rev. Lett.*, 1979, **43**, 1494–1497.

59 A. J. Morris, R. J. Nicholls, C. J. Pickard and J. R. Yates, OptaDOS: A tool for obtaining density of states, core-level and optical spectra from electronic structure codes, *Comput. Phys. Commun.*, 2014, **185**, 1477–1485.

60 R. J. Nicholls, A. J. Morris, C. J. Pickard and J. R. Yates, OptaDOS-a new tool for EELS calculations, *J. Phys.: Conf. Ser.*, 2012, **371**, 012062.

61 J. Lin, M. H. Lee, Z. P. Liu, C. T. Chen and C. J. Pickard, Mechanism for linear and nonlinear optical effects in β-BaB_2O_4 crystals, *Phys. Rev. B: Condens. Matter Mater. Phys.*, 1990, **60**, 13380–13389.

62 K. Momma and F. Izumi, VESTA3 for three-dimensional visualization of crystal, volumetric and morphology data, *J. Appl. Crystallogr.*, 2011, **44**, 1272–1276.

63 C. Deng, J. Wang, M. Hu, X. Cui, H. Duan, P. Li and M. H. Lee, Positive and Negative Contribution from Lead-Oxygen Groups and Halogen Atoms to Birefringence: A First Principles Investigation, *Nanomaterials*, 2023, **13**, 3037.

64 K. S. Lee, Y. U. Kwon, H. Namgung and S. H. Kim, A New Layered Mixed-Valent Potassium Vanadium Selenite, KV_2SeO_7, *Inorg. Chem.*, 1995, **34**, 4178–4181.

65 M. L. Liang, Y. X. Ma, C. L. Hu, F. Kong and J. G. Mao, A $(VO_2F)(SeO_3)$(A = Sr, Ba) and $Ba(MOF_2)(TeO_4)$(M = Mo, W): first examples of alkali-earth selenites/tellurites with a fluorinated d^0-TM octahedron, *Dalton Trans.*, 2018, **47**, 1513–1519.

66 Y. U. Kwon, K. S. Lee and Y. H. Kim, $AVSeO_5$ (A = Rb, Cs) and $AV_3Se_2O_{12}$ (A = K, Rb, Cs, NH4): Hydrothermal Synthesis in the V_2O_5-SeO_2-AOH System and Crystal Structure of $CsVSeO_5$, *Inorg. Chem.*, 1996, **35**, 1161.

67 Y. Shin, D. W. Lee, K. Y. Choi, H. J. Koo and K. M. Ok, $VSb(SeO_3)_4$, first selenite containing V^{3+} cation: synthesis, structure, characterization, magnetic properties, and calculations, *Inorg. Chem.*, 2013, **52**, 14224–14230.

68 S. Konatham and K. Vidyasagar, Syntheses and structural characterization of vanado-tellurites and vanadyl-selenites: $SrVTeO_5(OH)$, $Cd_2V_2Te_2O_{11}$, $Ca_3VSe_4O_{13}{\cdot}H_2O$ and $Ba_2VSe_3O_{10}$, *J. Solid State Chem.*, 2017, **249**, 39–45.

69 C. C. Jin, F. M. Li, B. L. Cheng, H. T. Qiu, Z. H. Yang, S. L. Pan and M. Mutailipu, Double–Modification Oriented Design of a Deep–UV Birefringent Crystal Functionalized by [$B_{12}O_{16}F_4(OH)_4$] Clusters, *Angew. Chem., Int. Ed.*, 2022, **61**, e202203984.

